https://doi.org/10.5194/egusphere-2024-1266
Preprint. Discussion started: 11 June 2024

Title page

Effect of colloidal particle size on physicochemical properties and aggregation behaviors of two alkaline soils

Yu-yang Yan[1], Xin-ran Zhang[1], Chen-yang Xu[1,2]*, Jun-jun Liu[1], Fei-nan Hu[3,4], Zeng-chao Geng[1,2]

(1. *College of Natural Resources and Environment, Northwest A&F University, Yangling, Shaanxi* 712100, *China*; 2. *Key Laboratory of Plant Nutrition and the Agri-environment in Northwest China, Ministry of Agriculture, Northwest A&F University, Yangling, Shaanxi 712100, China; 3. State Key Laboratory of Soil Erosion and Dryland Farming on the Loess Plateau, Northwest A&F University, Yangling, Shaanxi 712100, China; 4. Institute of Soil and Water Conservation, Chinese Academy of Sciences, Ministry of Water Resources, Yangling, Shaanxi 712100, China*)

***Corresponding author:**

Chen-yang Xu

Email address: xuchenyang@nwafu.edu.cn, xuchenyang.ms@163.com;

Postal address: College of Natural Resources and Environment, Northwest A&F University, No. 3 Taicheng Road, Yangling District, Shaanxi 712100, China.

https://doi.org/10.5194/egusphere-2024-1266
Preprint. Discussion started: 11 June 2024

Abstract

Soil colloidal particles are the most active components of all, and they also vary in elemental composition and environmental behaviors with the particle size. The purposes of the present study are to clarify how particle size affects the physiochemical properties and aggregation kinetics of soil colloids, and to further reveal the underlying mechanisms. Soil colloidal particles from two alkaline soils—Lou soil and cinnamon soil were subdivided into three ranges: $d < 2$ μm, $d < 1$ μm and $d < 100$ nm. The organic and inorganic carbon contents, clay mineralogy, surface electrochemical properties, including surface functional groups and zeta potentials, were characterized. Through time-resolved light scattering technique, the aggregation kinetics of soil colloidal fractions were investigated, and their critical coagulation concentrations (CCCs) were determined. With decreasing colloidal particle diameter, the total carbon content, organic carbon, organic functional groups content and illite content all increased. The absolute zeta potential values and the charge variability decreased with decreasing particle diameter. The CCC values of Lou soil and cinnamon soil colloids followed the descending order of $d < 100$ nm, $d < 1$ μm, $d < 2$ μm. Compared with the course factions ($d < 1$ μm and $d < 2$ μm), soil nanoparticles were more abundant in organic carbon and more stable clay minerals ($d < 100$ nm), thus they exhibited strongest colloidal suspension stability. The differences in organic matter contents and clay mineralogy are the fundamental reasons for the differences in colloidal suspension stability behind the size effects of Lou soil and cinnamon soil colloids. The present study revealed the size effects of two alkaline soil colloids on carbon content, clay minerals, surface properties

https://doi.org/10.5194/egusphere-2024-1266
Preprint. Discussion started: 11 June 2024

and suspension stability, emphasizing that soil nanoparticles are prone to be more stably dispersed instead of being aggregated. These findings can provide references for in-depth understanding of the environmental behaviors of the heterogeneous soil organic-mineral complexes.

Keywords: Nanoparticles; Clay mineral composition; zeta potential; Critical coagulation concentration

https://doi.org/10.5194/egusphere-2024-1266
Preprint. Discussion started: 11 June 2024

1. Introduction

Soils contain a series of solid particles in continuous sizes, ranging over six orders of magnitude from nanometers to millimeters (Lead and Wilkinson, 2006; Li et al., 2011), among which soil colloids are the most active parts. Soil colloids are characterized by high surface area and strong adsorption capacity, which can largely determine the fate and transport of pathogens, nutrients, heavy metals and organic pollutants, and might cause environmental problems to adjacent water bodies or groundwater (Baalousha et al., 2009). Due to their high reactivity and fluidity in aqueous environment, soil colloids play an important role in physical, chemical and biogeochemical processes of natural environment (Schäfer et al., 2012; Mayordomo et al., 2016). The capacity of soil colloids in driving attached nutrients and pollutants is closely related to their dispersion stability under various environmental conditions (Won and Burns, 2018). Therefore, studies on the dispersion stability of soil colloids have attracted extensive attention.

Currently, the definition of soil and environmental colloidal fractions is ambiguous. Soil colloidal fractions are defined as soil particles in diameter of < 1 μm (Lead and Wilkinson, 2006; Weil and Brady, 2016), and also being of < 2 μm (Zhang et al., 2021); while in some extreme cases, they can refer to the particles in diameter of 5–10 μm (Yin et al., 2010). Such discrepancies are seen among publications due to the fact that colloids are defined based on the particle diameter range within which they can display colloidal properties. Since for different materials, e.g., metal (Fe/Al/Ti) oxides, silica gel, phyllosilicates, the specific colloidal range differs greatly.

Compared with engineered nanoparticles with known mineralogical organization,

https://doi.org/10.5194/egusphere-2024-1266
Preprint. Discussion started: 11 June 2024

natural soils are much more heterogeneous (Cárdenas et al., 2010); their elemental composition and clay mineralogy of soil colloids change with particle size. Tsao et al., (2013) found that quartz and feldspar were mainly dominant in colloidal particles of < 2 μm and 450–2000 nm in red soil, while illite and montmorillonite were the main clay minerals in nanoparticles (1–100 nm). In addition, the mineral structure at nanometer scale also changes. Compared with colloidal particles of < 2 μm, the Si/Al ratio in nanoparticles increased, and the surface area, morphology, crystallinity, surface atomic structure and frame structure were significantly different (Tsao et al., 2011). Furthermore, particle size also affects the surface potential of soil colloids. Tang et al., (2015) investigated the surface potential variations with particle size (1–10 μm, 0.5–1 μm, 0.2–0.5 μm, < 0.2 μm) for variably-charged yellow soil and permanently-charged purple soil; among the colloidal fractions, the absolute surface potential of the finest particles of purple soil was lowest while that of the yellow soil was the largest, caused by the differences in surface charge density. Thus, the influences of particle size on elemental composition and surface properties of soils should be further studied.

In recent years, great progress has been made in the study of dispersion stability of soil clay minerals, such as montmorillonite, kaolinite, illite or hematite, and soil nanoparticles (Xu et al., 2018; Sun et al., 2020; Wei et al., 2021; Zhu et al., 2014). He et al., (2008) demonstrated that hematite nanoparticles with various particle diameters showed different surface properties and aggregation behaviors under the same pH conditions; moreover, the critical coagulation concentrations (CCCs) of hematite decreased with the decrease of particle diameter. Zhou et al., (2013) compared the

https://doi.org/10.5194/egusphere-2024-1266
Preprint. Discussion started: 11 June 2024

CCCs of ten different TiO_2 nanoparticles with varying sizes and indicated that crystal structure and particle diameter both affected the aggregation behaviors of TiO_2. Zhang et al. (2016) confirmed that the types of clay minerals for two Alfisols changed from smectite and vermiculite to kaolinite and illite when the particle size varied from colloids to nanoparticles. Therefore, the dependence of physiochemical properties, surface properties and environmental behaviors on particle size for heterogeneous soil colloidal particles needs systematic investigation.

In the present study, soil colloidal particles of two alkaline soils—Lou soil and cinnamon soil were subdivided into three ranges: $d < 2$ μm, $d < 1$ μm and $d < 100$ nm. Their organic fraction and clay mineralogy, surface electrochemical properties and colloidal stability were studied. The objectives of the present study are to clarify how particle size affects the surface properties and aggregation behaviors of soil colloids, and to analyze the underlying mechanisms. The findings are of important significances for predicting the environmental performances of colloids and colloid-facilitated nutrients, pollutes and pathogens in natural soil and water environment.

2. Materials and methods

2.1 Soil sampling

Two representative surface soils (0–20 cm) were collected from the Guanzhong Plain, China, namely Lou soil (agricultural soil) and cinnamon soil (natural soil). Lou soil was collected from Yangling District, Shaanxi Province. Cinnamon soil was collected from Zhouzhi County, Shaanxi Province. Lou soil and cinnamon soil are classified as Anthrosols and Calcisols, respectively, according to the FAO soil

https://doi.org/10.5194/egusphere-2024-1266
Preprint. Discussion started: 11 June 2024

classification. Soils were taken back to laboratory for air-drying and sieving. The basic soil properties are determined based on standard methods. The pH of Lou soil was 8.34 while it was 8.32 for the cinnamon soil. The organic carbon contents of Lou soil and cinnamon soil were 7.25 $g \cdot kg^{-1}$ and 9.22 $g \cdot kg^{-1}$, respectively. The contents of $CaCO_3$ in Lou soil and cinnamon soil were 51.7 $g \cdot kg^{-1}$ and 82.5 $g \cdot kg^{-1}$. The Free Fe/Al oxides content of Lou soil and cinnamon soil were 22.8 $g \cdot kg^{-1}$ and 23.1 $g \cdot kg^{-1}$.

2.2 Extraction of soil colloidal fractions in different size ranges

The soil colloidal particles were extracted based on the Stokes' law, and the detailed procedures can be found in our previous publication (Hu et al., 2022). Briefly, weigh 50 g soil into a beaker containing 500 mL distilled water, and put the suspension under sonication for an hour using the ultrasonic cell disrupter (XO-900D, Nanjing Xianou Instruments Corporation, China) while maintaining the temperature below 30°C. Afterwards, the suspension was transferred to a larger beaker and distilled water was added to make up the total volume of 5 L. The suspension was further dispersed using an electronic blade stirrer (JB-200, Shanghai Nanhui Huiming Apparatus, China) for one hour, before being sifted through a 300-mesh sieve, and the upper suspensions containing soil colloidal particles in different diameters were collected by centrifugation. Based on the equation (1), centrifugation speed and time for colloidal particles of $d < 2$ μm, < 1 μm and < 100 nm are calculated and shown in Table S1.

$$t = \frac{\eta \lg \frac{R_2}{R_1}}{3.81 N^2 r^2 \Delta d} \quad (1)$$

in which, t is time for centrifugation (s); R_1 is the distance from the surface of the liquid

https://doi.org/10.5194/egusphere-2024-1266
Preprint. Discussion started: 11 June 2024

to the center of the axis of the centrifuge, here is 5.7 cm; R_2 is distance from the particles to the center of the axis of the centrifuge, here is 10.5 cm; N (rev·s^{-1}) is the centrifuge speed; r (cm) is the desired colloidal particle radius; Δd is the difference in density between the soil particles and water, while Δd is 1.65 g·cm^{-3}; η is the water viscosity coefficient, here is 0.00839 g·cm^{-1}·s^{-1} at 25 °C.

2.3 Characterization of soil colloidal fractions in different size ranges

The initial particle diameters of soil colloids were determined by a time-resolved dynamic light scattering (DLS) apparatus (Nanobrook Omni, Brookhaven, USA). The organic carbon contents in soil colloids were determined by potassium dichromate external heating method and total carbon content was determined by elemental analyzer (Elementar Vario EL III, Germany). The inorganic carbon content was calculated by subtraction method (Wang et al., 2011). The clay mineralogy of soil colloids was determined by the XRD (Ultima-IV, Rigaku, Japan). The specific surface areas of the soil colloids were measured by BET-N_2 method (ASAP 2460, Micromeritics instrument, USA). High-resolution spectra of C1s and O1s of soil colloids were acquired by X-ray photoelectron spectroscopy (XPS) (Thermo Scientific K-Alpha, USA) (Luo et al., 2019). The zeta potentials of soil colloids were measured by Zeta PALS equipped with a BI-ZTU Autotitrator (ZetaPALS, Brookhaven, USA) with 1 mmol·L^{-1} NaCl solution as the background electrolyte; and the pH range of colloidal suspension was set to 3–10 adjusted with 0.1 mol·L^{-1} HCl and NaOH. The concentrations of K^+, Na^+, Ca^{2+}, and Mg^{2+} in soil colloidal suspensions were measured by flame atomic absorption spectrophotometry (PinAAciie 900F, USA).

https://doi.org/10.5194/egusphere-2024-1266
Preprint. Discussion started: 11 June 2024

2.4 Aggregation kinetics of soil colloidal fractions

The aggregation kinetic curves of soil colloidal particles in different electrolytes were determined by time-resolved DLS measurements. The incident wavelength was 635 nm and the scattering angle was 90°. While using the DLS instrument, it is necessary to clean up the surrounding dust, especially the sample pool. The stock colloidal suspensions with particle concentration of 200 $mg \cdot L^{-1}$ were mixed with electrolyte solutions with equal volume. The suspension pH was adjusted to 8.0, which was close to the pH value of natural soil with addition of 0.1 $mol \cdot L^{-1}$ HCl or NaOH before measurement. The chosen electrolyte concentrations for NaCl and $CaCl_2$ were 200–2000 and 2–20 $mmol \cdot L^{-1}$. The effective diameter (D_h) of the mixed sample was automatically recorded every 2 min, and an aggregation kinetic curve was obtained in 30 min monitoring.

2.5 Calculation of critical coagulation concentration

According to the particle interaction theory, the aggregation kinetic curves under electrolyte conditions can be divided into reaction-limited aggregation (RLA) stage under low concentration which was affected by electrolyte conditions and diffusion-limited aggregation (DLA) stage under high concentration which was not affected by electrolyte concentration. The CCC is the critical electrolyte concentration when the aggregation process changes from the RLA state ($\alpha < 1$) to the DLA state ($\alpha = 1$). Attachment efficiency (α) represents the bonding probability of particle collisions and can be calculated for each electrolyte concentration by using equation 2, which allowed the curve of α as a function of electrolyte concentration to be plotted (Xu et al., 2020a;

https://doi.org/10.5194/egusphere-2024-1266
Preprint. Discussion started: 11 June 2024

Hu et al., 2022).

$$\alpha_{exp} = \frac{1}{W} = \frac{k_{11}}{(k_{11})_{fast}} = \frac{\frac{1}{N_0}\left(\frac{da_h(t)}{dt}\right)_{t\to 0}}{\frac{1}{(N_0)_{fast}}\left(\frac{da_h(t)}{d_t}\right)_{t\to 0,\,fast}} \quad (2)$$

where D_h is the effective diameter of particles, t is the time (min); N_0 is the density of particles; K_{11} is the aggregation rate of RLA; $(K_{11})_{fast}$ is the aggregation rate of DLA. The intersection of RLA regime and DLA regime is the CCC.

The aggregation rates were calculated by the average of the last 5 effective diameters divided by the aggregation time at specific electrolyte concentration. The fractal dimension in the DLA regime was obtained based on the method proposed by Wang et al. (2013).

$$D(t) = b * t^n + D_0 \quad (3)$$

in which, $D(t)$ is the colloidal effective diameter at time t (min), D_0 is the initial effective diameter of colloids, and b and n are constants determined by the aggregation curves. The fractal dimension is $d_f = 1/n$ in the DLA regime.

3. Results and discussion

3.1 Particle size and distribution characteristics of Lou soil and cinnamon soil colloidal fractions

The average diameters of Lou soil and cinnamon soil colloids were measured by time-resolved DLS, and the results were shown in Table 1. The number-weighted diameters for Lou soil colloids of $d < 2$ μm, < 1 μm and < 100 nm were 133.16, 127.84 nm and 72.47 nm, respectively. The intensity-weighted diameters were 396.81 nm,

https://doi.org/10.5194/egusphere-2024-1266
Preprint. Discussion started: 11 June 2024

371.45 nm and 294.10 nm. For cinnamon soil colloidal fractions, the number-weighted diameters for colloids of $d < 2$ μm, < 1 μm and < 100 nm were 141.23 nm, 131.67nm and 85.48 nm, and their intensity-weighted diameters were 439.20 nm, 372.07nm and 312.25 nm, respectively. The intensity-weighted diameters were generally higher than the number-weighted diameters, especially in polydisperse system (Xu et al., 2020b). The particles in the soil solution are in constant Brownian motion, and when light passes through the colloids, the particles will undergo light scattering, resulting in fluctuations in light intensity, and thus the effective diameter (intensity-weighted diameter) of the particles is calculated (Filella et al., 1997). Since the particle diameter is proportional to the sixth power of the light intensity, that is, if there are larger particles in the solution in such polydisperse systems, the number-weighted diameter is generally more representative of the true diameter of colloidal particles (Xu et al., 2015).

(*Insert Table 1 near here*)

From table 1, it can be seen that the average colloidal diameters of $d < 2$ μm were close to that of $d < 1$ μm, and they were both significantly higher that of the nano-sized fraction. From the particle size distribution characteristics, it is clear that the size range indicated by the differences of D_{90} and D_{10} increased with intended particle diameter. For Lou soil and cinnamon soil, 74.69% and 63.55% of all particles contained in the colloidal suspensions of $d < 100$ nm were actually less than 100 nm, respectively, indicating the complexity of soil colloidal particle irregularity.

https://doi.org/10.5194/egusphere-2024-1266
Preprint. Discussion started: 11 June 2024

3.2 Physiochemical properties and clay mineralogy of Lou soil and cinnamon soil colloids

Table 2 shows the physiochemical properties of soil colloidal fractions. The yields of each colloidal fraction of Lou soil were slightly larger than that of cinnamon soil, respectively. The yields of colloidal particles of $d < 2$ μm were about 1.3~1.4 times of $d < 1$ μm, and about 4.0~4.9 times of $d < 100$ nm, respectively. With the decreasing colloidal particle diameter, the total carbon content, organic carbon and inorganic carbon content all increased, suggesting the finer particles were richer in carbon. This tendency is in agreement with other publications (Zhang et al., 2021; Said-Pullicino et al., 2021; Hu et al., 2022). The specific surface areas for colloidal fractions of $d < 1$ μm were largest of all, which may be related to the structures of formed clusters while drying the samples for observation under microscopy (Yu et al., 2017; Weissenberger et al., 2021).

(*Insert Table 2 near here*)

The clay mineralogy of Lou soil and cinnamon colloidal fractions is shown in Table 3. Cinnamon soil colloidal fractions were dominant by illite, kaolinite and chlorite while there was less chlorite in Lou soil colloidal fractions. With the decrease of particle size, the content of illite increased and kaolinite content decreased. This tendency is in agreement with other publications (Chenu and Plante, 2006; Zhang et al., 2016). Among the dominant clay types, the size of illite is finer than kaolinite and chlorite (Weil and Brady, 2016), so its mass percentage was higher in the nano-sized fraction.

https://doi.org/10.5194/egusphere-2024-1266
Preprint. Discussion started: 11 June 2024

(*Insert Table 3 near here*)

3.3 Surface properties of Lou soil and cinnamon soil colloids

The XPS spectra of soil colloidal fractions are shown in Fig. 1. From Fig. 1, it can be seen that the main C-containing functional groups were C–C/C-H/C=C, C–O, C=O, and COO- groups at 284.6, 286.2, 288.0 and 289.4 eV, respectively (Liang et al., 2020; Ding et al., 2023). The functional groups for colloidal particles of d < 100 nm were more abundant than those for colloids of d < 2 μm and d < 1 μm, while there were no significant differences between colloids of d < 2 μm and d < 1 μm. With the decrease of colloidal particle diameter, the relative contents of oxygen-containing functional groups (C–O, C=O, COO-) gradually decreased. Specifically, the content decreased gradually from 32.01% in Lou colloids of d < 2 μm to 20.93% in Lou colloids of d < 100 nm (Table S2). The functional groups of C–O and COO- gradually decreased until they eventually disappeared, more C=O groups were exposed to the surrounding air.

For cinnamon soil colloids (Fig. 1d, e, f), the relative contents of organic oxygen-containing functional groups for colloidal particles of d < 2 μm, d < 1 μm and d < 100 nm showed a different trend, compared with that in Lou soil colloids. The relative contents of organic oxygen-containing functional groups gradually increased with the decrease of diameter. This trend was particularly pronounced in fraction of d < 100 nm, and contents of C–O and COO- were highly increased (Table S2).

(*Insert Figure 1 near here*)

Oxygen-containing functional groups of C–O, C=O and COO- are electronegative functional groups, hydroxyl and carboxyl groups can lose protons and make the surface of soil colloidal particles carry negative charges (Audette et al., 2021). Functional groups of C–O, C=O and COO- can affect the negative charges carried on the colloidal

https://doi.org/10.5194/egusphere-2024-1266
Preprint. Discussion started: 11 June 2024

surface by forming hydrogen bonds, and their polarity can also affect the negative charges on the surface when O atom combines with C and H. The electrons will lean towards the O atom with stronger electronegativity, which also makes the colloidal surface carry negative charges (Tan et al., 2019). The contents and types of oxygen-containing functional groups are one of the main factors affecting colloid charge and aggregation.

The zeta potential values of different colloidal fractions at the pH range of 3–10 are shown in Fig. 2. Zeta potentials of the colloidal particles were negative, indicating that they were negatively-charged. The absolute values of zeta potentials for of Lou soil and cinnamon soil colloidal particles increased with increasing solution pH, due to the deprotonation of the surface (Moayedi and Kazemian, 2013; Dong et al., 2019). Compared with the cinnamon soil colloids, the zeta potentials of Lou soil colloidal particles were more negative. For cinnamon soil colloids, the differences among colloidal fractions were larger.

(*Insert Figure 2 near here*)

In general, the absolute zeta potential values increased with increasing particle diameter. When the pH changed from 3 to 10, for every pH unit increased, the zeta potential values of Lou soil colloids of d < 2 μm, < 1 μm, and < 100 nm would be increased by 2.14 mV, 2.09 mV and 1.89 mV; and for cinnamon soil colloids, those variation rates were 2.15 mV, 1.45 mV and 1.37 mV, respectively. Those data demonstrate that the charge variability decreasing with the decreasing particle diameter. Song et al., (2019) compared the zeta potential of wheat straw biochar nanoparticles (<

https://doi.org/10.5194/egusphere-2024-1266
Preprint. Discussion started: 11 June 2024

100 nm) and colloidal particles (< 1000 nm), and found that the absolute values of colloidal particles were larger at same pH, which was explained by the differences in the number of surface carboxyl and hydroxyl groups. The zeta potential of colloidal particles is proportional to charge density, which means that it is related to both charge quantity and specific surface area (Hou et al., 2009). Therefore, the size effect of zeta potential of Lou soil and cinnamon soil colloidal particles is mainly related to the reduction of charge density caused by larger specific surface area of nanoparticles (Xu et al. 2020b).

3.4 Aggregation kinetics curves of Lou soil and cinnamon soil colloids in NaCl and $CaCl_2$ solutions

The aggregation kinetics of Lou soil and cinnamon soil colloids in NaCl and $CaCl_2$ solutions are shown in Figs. S1 and S2. The aggregation process of soil colloids was divided into RLA and DLA stages. The RLA stages for Lou soil colloids of d < 2 μm, d < 1 μm and d < 100 nm in NaCl solution were 0–80, 0–80 and 0–100 mmol·L^{-1}, respectively, during which repulsive forces existed between the particles and attachment did not occur on every collision. As the electrolyte concentration continued to increase, the solution entered into the DLA regime. At this point, attachment occurred with every collision between particles, and the aggregation rates were not affected by the electrolyte concentration. At last, the effective diameters of the formed clusters were stable at around 1600 nm. Figure S1b, d and f showed that the aggregation behaviors of Lou soil colloids in $CaCl_2$ solution were similar to that in NaCl solution, and the corresponding $CaCl_2$ concentrations for Lou soil colloids of d < 2 μm, d < 1 μm and d

https://doi.org/10.5194/egusphere-2024-1266
Preprint. Discussion started: 11 June 2024

< 100 nm in RLA stage were about 0–1.5, 0–1.5 and 0–2 mmol·L^{-1}, respectively.

The aggregation kinetics of cinnamon soil colloids in NaCl and $CaCl_2$ solutions were similar to Lou soil colloids (Fig. S2). The RLA stages for cinnamon soil colloids of d < 2 μm, d <1 μm and d <100 nm in NaCl solution were 0–100, 0–120 and 0–250 mmol·L^{-1}, and were about 0–1.8、0–1.7 and 0–2 mmol·L^{-1} in $CaCl_2$ solution, respectively. The effective diameters of the clusters for cinnamon soil colloids were stabilized at about 1600 nm and 1800 nm in NaCl and $CaCl_2$ solutions, respectively.

Aggregation rates of soil colloids varied with particle diameters at the same electrolyte concentration, which was particularly evident in RLA stage (Table 4). For Lou soil colloids of d < 2 μm, d < 1 μm and d < 100 nm with addition of 50 mmol·L^{-1} NaCl, aggregation rates were 19.46, 14.91 and 7.22 nm·min^{-1}, respectively, while those of cinnamon soil colloids were 8.98, 7.15 and 3.95 nm·min^{-1} with decreasing particle diameter. In 1 mmol·L^{-1} $CaCl_2$ solution, the aggregation rates of cinnamon soil colloids of d < 2 μm, d < 1 μm and d < 100 nm were 8.22, 7.33 and 5.22 nm·min^{-1}, respectively. Therefore, from table 4, the aggregation rates of Lou soil and cinnamon soil colloids showed the size effect. From table 4, it could be observed that the fractal dimensions in NaCl solutions were largely higher than those in $CaCl_2$ solutions, suggesting a much denser structure (Meng et al., 2013). In other words, the formed structures in divalent solutions were more open.

(*Insert Table 4 near here*)

https://doi.org/10.5194/egusphere-2024-1266
Preprint. Discussion started: 11 June 2024

3.5 Suspension stability of Lou soil and cinnamon soil colloids in NaCl and $CaCl_2$ solutions

The CCCs for Lou soil colloids of $d < 2$ μm, $d < 1$ μm and $d < 100$ nm in NaCl solution were 80.40, 91.78 and 134.96 mmol·L^{-1}, respectively (Fig. 3a), and those for cinnamon soil colloids were 121.10, 126.50 and 292.86 mmol·L^{-1}, respectively (Fig. 3b). The CCCs increased with the decreasing particle diameter, indicating that the suspension stability of soil nanoparticles was stronger than those of colloidal particles.

(*Insert Figure 3 near here*)

In $CaCl_2$ solutions, the CCCs for Lou soil colloids of $d < 2$ μm, $d < 1$ μm and $d < 100$ nm were 1.61, 1.68 and 1.77 mmol·L^{-1}, respectively, and for cinnamon soil colloids, those corresponding values were 1.90, 1.91 and 2.13 mmol·L^{-1} (Fig. 4). The CCCs in $CaCl_2$ solutions also increased with the decreasing particle size. The contents of K^+, Na^+, Ca^{2+} and Mg^{2+} in Lou soil and cinnamon soil colloidal suspensions decreased with the decreasing colloidal particle diameter (Table S3), which was mainly due to the dilution effect during the extraction process. Furthermore, Table S3 showed that the soluble cation contents were rather low, and their effects on the CCCs of soil colloids could be neglected.

(*Insert Figure 4 near here*)

Based on Figs. 3 and 4, 3 mmol·L^{-1} $CaCl_2$ solution could cause fast aggregation of soil colloidal particles, while it required at least 80 mmol·L^{-1} NaCl solution for comparable aggregation rate, indicating that the shielding effect of divalent cations on negative charges of colloids was stronger than that of monovalent cations. The

https://doi.org/10.5194/egusphere-2024-1266
Preprint. Discussion started: 11 June 2024

quantitative calculation results showed that the CCC ratios of monovalent ion and divalent ion system were between 25.64 and 27.09, which conformed to the Schulze-Hardy rule (Baalousha, 2017).

For each type of the soil colloids, the higher the absolute zeta potential values of colloidal particles, the more negative charges carried on the surface, and the higher the stability (CCCs) of suspension. For the same particle diameter, e.g. d < 100 nm, the absolute zeta potentials of Lou soil colloids were larger (Fig. 2) while the corresponding CCC was lower (Figs. 3 and 4). Study on the stability of biochar nanoparticles showed that the absolute values of zeta potentials could not be used to directly explain the stability difference among biochar nanoparticles from different feedstock materials but could explain the influences of solution conditions on the stability of biochar nanoparticles derived from the same feedstock material (Xu et al., 2020a).

The CCCs of Lou soil and cinnamon soil colloids increased with decreasing diameter; that is, the CCCs of Lou soil and cinnamon soil colloids both showed the size effects. Hsu and Kuo (1995) demonstrated that the CCCs would generally decrease with the increasing particle diameter because smaller particles possess thicker double electric layers and higher electrolyte concentration is needed to neutralize charges on the surface, which were consistent with the results of Lou soil and cinnamon soil colloids. The above explanation by Hsu and Kuo (1995) was derived from homogenous particles whose composition does not change with particle diameter. The results of this paper show that, for those two alkaline soils being such heterogeneous materials, when the organic matter contents and mineral types changed with colloidal particle diameter,

https://doi.org/10.5194/egusphere-2024-1266
Preprint. Discussion started: 11 June 2024

the CCCs in monovalent and divalent solutions also decreased with increasing particle diameter.

In this paper, the organic matter contents of soil nanoparticles were the highest, so the CCCs were the largest, which were 1.7 and 2.4 times of the corresponding colloidal particles of $d < 2$ μm. The suspension stability of different clay minerals has been reported to vary with the mineralogical structure. The CCC of illite (≈100 mM) in NaCl solution was significantly higher than that of kaolinite (≈20 mM) (Jiang et al., 2012; Xu et al., 2017). Another possible reason for the higher stability of soil nanoparticles is the increase of illite content and the decrease of kaolinite content. Therefore, the differences in organic matter contents and clay mineralogy are the fundamental reasons for the differences in colloidal suspension stability behind the size effects of Lou soil and cinnamon soil colloids.

4. Conclusion

The size effect of heterogeneous soil colloidal particles was demonstrated. The number-weighted diameters for Lou soil and cinnamon soil colloids of $d < 100$ nm were 72.47 nm and 85.48 nm, respectively. With the decreasing colloidal particle diameter, the total carbon content, organic carbon, organic functional groups content and illite all increased, indicating the finer particle size of the organic faction and illite. The absolute zeta potential values and the charge variability decreased with the decreasing particle diameter. Aggregation rates of soil colloids decreased with the decreasing of particle diameter at the same electrolyte concentration, which was particularly evident in RLA stage. In NaCl or $CaCl_2$ solution, the CCCs increased with the decreasing Lou soil and

https://doi.org/10.5194/egusphere-2024-1266
Preprint. Discussion started: 11 June 2024

cinnamon soil colloidal particle diameter, indicating that the suspension stability was enhanced. These findings have important implications for predicting the environmental behaviors of soil colloids and related colloid-facilitated nutrient/contaminant transport.

Acknowledgments

This work was supported by Natural Science Foundation of Shaanxi Province (2023-JC-YB-263) and the National Natural Science Foundation of China (41701261), and the Fundamental Research Funds for the Central Universities (2452020165).

Author Contributions

Conceptualization, Xu, C.Y., Geng, Z.C., and Hu, F.N.; methodology, Xu, C.Y.; software, Yan, Y.Y.; formal analysis, Liu, J.J.; investigation, Zhang, X.R.; resources, Yan, Y.Y.; writing—original draft, Yan, Y.Y.; writing—review and editing, Xu, C.Y., and Hu, F.N.; visualization, Xu, C.Y., and Yan, Y.Y.; funding acquisition, Xu, C.Y., Geng, Z.C. and Hu, F.N.. All authors have read and agreed to the published version of the manuscript.

Declaration of Interest Statement

The authors declare that they have no known competing financial interests or personal relationships that could have appeared to influence the work reported in this paper.

https://doi.org/10.5194/egusphere-2024-1266
Preprint. Discussion started: 11 June 2024

References

Audette, Y., Congreves, K.A., Schneider, K., Zaro, G.C., Nunes, A.L.P., Nunes, A.L.P., Zhang, H.J., Voroney, R.P.: The effect of agroecosystem management on the distribution of C functional groups in soil organic matter: A review. Biol. Fertil. Soils. 57, 881–894, 2021.

Baalousha, M.: Aggregation and disaggregation of iron oxide nanoparticles: Influence of particle concentration, pH and natural organic matter. Sci. Total Environ. 407(6), 2093–2101, 2009.

Baalousha, M.: Effect of nanomaterial and media physicochemical properties on nanomaterial aggregation kinetics. NanoImpact. 6, 55–68, 2017.

Cárdenas, J.P., Santiago, A., Tarquis, A.M., Losada, J.C., Borondo, F., Benito, R.M.: Soil porous system as heterogeneous complex network. Geoderma. 160(1), 13–21, 2010.

Chenu, C., Plante, A.F.: Clay-sized organo-mineral complexes in a cultivation chronosequence: revisiting the concept of the‘primary organo-mineral complex’. Eur J Soil Sci. 57(4), 596–607, 2006.

Ding, W., Liang, H.X., Zhang, H.W., Sun, H., Geng, Z.C., Xu, C.Y.: A cellulose/bentonite grafted polyacrylic acid hydrogel for highly-efficient removal of Cd(II). J. Water Process. Eng. 51, 103414, 2023.

Dong, S.N., Zeng, Z., Cai, W.W., Zhou, Z.Y., Dou, C.B., Liu, H., Xia, J.H.: The zeta potentials of g-C_3N_4 nanoparticles: Effect of electrolyte, ionic strength, pH, and

https://doi.org/10.5194/egusphere-2024-1266
Preprint. Discussion started: 11 June 2024

humic acid. J. Nanopart Res. 21, 233, 2019.

Filella, M., Zhang, J.W., Newman, M.E., Buffle, J.: Analytical applications of photon correlation spectroscopy for size distribution measurements of natural colloidal suspensions: capabilities and limitations. Colloid Surf. A. 120(1–3), 27–46, 1997.

He, Y.T., Wan, J., Tokunaga, T.: Kinetic stability of hematite nanoparticles, The effect of particle sizes. J. Nanopart Res. 10, 321–332, 2008.

Hou, J., Li, H., Zhu, H.L.,Wu, L.S.: Determination of clay surface potential, a more reliable approach. Soil Sci Soc Am J. 73(5), 1658–1663, 2009.

Hsu, J.P., Kuo, Y.C.: An Extension of the Schulze-Hardy Rule to Asymmetric Electrolytes. J. Colloid Interface Sci. 171(1), 254–255, 1995.

Hu, N., Xu, C.Y., Geng, Z.C., Hu, F.N., Li, Q.R., Ma, R.T., Wang, Q.: The interplay of particle properties and solution chemistry on aggregation kinetics of soil nanoparticles. J Soils Sediments. 22, 1761–1772, 2022.

Jiang, C.L., Séquaris, J.M., Vereecken, H., Klumpp, E.: Effects of inorganic and organic anions on the stability of illite and quartz soil colloids in Na-, Ca- and mixed Na-Ca systems. Colloids Surf. A. 415, 134–141, 2012.

Lead, J.R., Wilkinson, K.J.: Aquatic Colloids and Nanoparticles: Current Knowledge and Future Trends. Environ. Chem. 3(3), 159–171, 2006.

Li, S.X., Luo, Y.M., Zhang, H.B., Huang, Y.J., Li, Z., Wei, J.: Arsenic forms in various particle-size fractions of red soil-Chemical fractionation and speciation using XANES analysis. Acta Scientiae Circumstantiae. 31(12), 2733–2739, 2011.

Liang, H.X., Sun, R.R., Song, B., Sun, Q.Q., Peng, P., She, D.: Preparation of nitrogen-

https://doi.org/10.5194/egusphere-2024-1266
Preprint. Discussion started: 11 June 2024

doped porous carbon material by a hydrothermal-activation two-step method and its high-efficiency adsorption of Cr(VI). J. Hazard. Mater. 387, 121987, 2020.

Luo, J.J., Niu, Q., Jin, M.C., Cao, Y.A., Ye, L.R., Du, R.P.: Study on the effects of oxygen-containing functional groups on Hg^0 adsorption in simulated flue gas by XAFS and XPS analysis. J. Hazard. Mater. 376(15), 21–28, 2019.

Mayordomo, N., Degueldre, C., Alonso, U., Missana, T.: Size distribution of FEBEX bentonite colloids upon fast disaggregation in low-ionic strength water. Clay Miner. 51(2), 213–222, 2016.

Meng, Z.Y., Hashmi, S.M., Elimelech, M.: Aggregation rate and fractal dimension of fullerene nanoparticles via simultaneous multiangle static and dynamic light scattering measurement. J. Colloid Interface Sci. 392, 27–33, 2013.

Moayedi, H., Kazemian, S.: Zeta potentials of suspended humus in multivalent cationic saline solution and its effect on electro-osomosis behavior. J. Dispers Sci. Technol. 34(2), 283–294, 2013.

Said-Pullicino, D., Giannetta, B., Demeglio, B., Missong, A., Gottselig, N., Romani, M., Bol, R., Klumpp, E., Celi, L.: Redox-driven changes in water-dispersible colloids and their role in carbon cycling in hydromorphic soils. Geoderma. 385, 114894, 2021.

Schäfer, T., Huber, F., Seher, H., Missana, T., Alonso, U., Kumke, M., Eidner, S., Claret, F., Enzmann, F.: Nanoparticles and their influence on radionuclide mobility in deep geological formations. Appl. Geochemistry. 27(2), 390–403, 2012.

Song, B.Q., Chen, M., Zhao, L., Qiu, H., Cao, X.D.: Physicochemical property and

https://doi.org/10.5194/egusphere-2024-1266
Preprint. Discussion started: 11 June 2024

colloidal stability of micron- and nano-particle biochar derived from a variety of feedstock sources. Sci. Total Environ. 661, 685–695, 2019.

Sun, Y.L., Pan, D.Q., Wei, X.Y., Xian, D.F., Wang, P., Hou, J.J.: Insight into the stability and correlated transport of kaolinite colloid: Effect of pH, electrolytes and humic substances. Environ. Pollut. 266, 115189, 2020.

Tan, Z.X., Yuan, S.N., Hong, M.F., Zhang, L.M., Huang, Q.Y.: Mechanism of negative surface charge formation on biochar and its effect on the fixation of soil Cd. J. Hazard. Mater. 384, 121370, 2019.

Tang, Y., Li, H., Liu, X.M., Zhu, H.L., Tian, R.: Unraveling the size distributions of surface properties for purple soil and yellow soil. J Environ Sci (China). 32, 81–89, 2015.

Tsao, T.M., Chen, Y.M., Sheu, H., Tzou, Y.M., Chou, Y.M., Wang, M.K.: Separation and identification of soil nanoparticles by conventional and synchrotron X-ray diffraction. Appl. Clay Sci. 85, 1–7, 2013.

Tsao, T.M., Chen, Y.M., Wang, M.K., Huang, P.M.: Structural transformation and physicochemical properties of environmental nanoparticles by comparison of various particle-size fractions. Soil Sci Soc Am J. 75(2), 533–541, 2011.

Wang, L.F., Wang, L.L., Ye, X.D., Li, W.W., Ren, X.M., Sheng, G.P., et al.: Coagulation kinetics of humic aggregates in mono-and divalent electrolyte solutions. Environ. Sci. Technol. 47(10), 5042–5049, 2013.

Wang, Q.R., Li, Y.C., Wang, Y.: Optimizing the weight loss-on-ignition methodology to quantify organic and carbonate carbon of sediments from diverse sources.

https://doi.org/10.5194/egusphere-2024-1266
Preprint. Discussion started: 11 June 2024

503 Environ. Monit. Assess. 174, 241–257, 2011.
504 Wei, X.Y., Pan, D.Q., Xu, Z., Xian, D.F., Li, X.L., Tan, Z.Y., Liu, C.L., Wu, W.S.:
505 Colloidal stability and correlated migration of illite in the aquatic environment:
506 The roles of pH, temperature, multiple cations and humic acid. Sci. Total Environ.
507 768, 144174, 2021.
508 Weil, R.R., Brady, N.C.: The Nature and Properties of Soils, Global Edition. Pearson
509 Education Limited. 2016.
510 Weissenberger, G., Henderikx, R.J., Peters, P.J.: Understanding the invisible hands of
511 sample preparation for cryo-EM. Nat. Methods. 18(5), 463–471, 2021.
512 Won, J., Burns, S.E.: Role of Immobile Kaolinite Colloids in the Transport of Heavy
513 Metals. Environ. Sci. Technol. 52(5): 2735–2741, 2018.
514 Xu, C.Y., Deng, K.Y., Li, J.Y., Xu, R.K.: Impact of environmental conditions on
515 aggregation kinetics of hematite and goethite nanoparticles. J. Nanopart Res. 17,
516 394, 2015.
517 Xu, C.Y., Li, Q.R., Geng, Z.C., Hu, F.N., Zhao, S.W.: Surface properties and suspension
518 stability of low–temperature pyrolyzed biochar nanoparticles: Effects of solution
519 chemistry and feedstock sources. Chemosphere. 259, 127510, 2020a.
520 Xu, C.Y., Xu, R.K., Li, J.Y., Deng, K.Y.: Phosphate-induced aggregation kinetics of
521 hematite and goethite nanoparticles. J. Soils Sediments. 17, 352–363, 2017.
522 Xu, C.Y., Zhou, T.T., Wang, C.L., Liu, H.Y., Zhang, C.T., Hu, F.N., Zhao, S.W., Geng,
523 Z.C.: Aggregation of polydisperse soil colloidal particles: Dependence of
524 Hamaker constant on particle size. Geoderma. 359, 113999, 2020b.

https://doi.org/10.5194/egusphere-2024-1266
Preprint. Discussion started: 11 June 2024

525 Xu, Z., Pan, D.Q., Sun, Y.L., Wu, W.S.: Stability of GMZ bentonite colloids:
526 Aggregation kinetic and reversibility study. Appl. Clay Sci. 161, 436–443. 2018.
527 Yin, X.Q., Gao, B., Ma, L.Q., Saha, U.K., Sun, H.M., Wang, G.D.: Colloid-facilitated
528 Pb transport in two shooting-range soils in Florida. J. Hazard. Mater. 177(1–3),
529 620–625, 2010.
530 Yu, X., Fu, Y., Lu, S.: Characterization of the pore structure and cementing substances
531 of soil aggregates by a combination of synchrotron radiation X-ray micro–
532 computed tomography and scanning electron microscopy. Eur. J. Soil Sci. 68(1),
533 66–79, 2017.
534 Zhang, Q., Bol, R., Amelung, W., Missong, A., Siemens, J., Mülder, I.: Water
535 dispersible colloids and related nutrient availability in Amazonian Terra Preta soils.
536 Geoderma. 397, 115103, 2021.
537 Zhang, Z.Y., Huang, L., Liu, F., Wang, M.K., Fu, Q.L., Zhu, J.: Characteristics of clay
538 minerals in soil particles of two Alfisols in China. Appl. Clay Sci. 120, 51–60,
539 2016.
540 Zhou, D.X., Ji, Z.X., Jiang, X.M., Dunphy, D.R., Brinker, J., Keller A.A.: Influence of
541 material properties on TiO_2 nanoparticle agglomeration. PLoS One. 8(11), e81239,
542 2013.
543 Zhu, X., Chen, H., Li, W., He, Y., Brookes, P.C., Xu, J.: Aggregation kinetics of natural
544 soil nanoparticles in different electrolytes. Eur. J. Soil Sci. 65(2), 206–217, 2014.
545
546

https://doi.org/10.5194/egusphere-2024-1266
Preprint. Discussion started: 11 June 2024

Table captions

Table 1 The average diameters and distribution patterns of Lou soil and cinnamon soil colloids.

Table 2 The physiochemical properties of Lou soil and cinnamon soil colloids.

Table 3 The dominant clay minerals of Lou soil and cinnamon soil colloidal fractions (shown in mass fraction, %).

Table 4 The aggregation rates of Lou soil and cinnamon soil colloids.

https://doi.org/10.5194/egusphere-2024-1266
Preprint. Discussion started: 11 June 2024

554 **Table 1** The average diameters and distribution patterns of Lou soil and cinnamon soil
555 colloids

Soil colloids	Colloidal fractions	Number-weighted diameter (nm)	Intensity-weighted diameter (nm)	D_{10} (nm)	D_{90} (nm)
Lou soil colloids	d < 2 μm	133.16	396.81	71.53	232.49
	d < 1 μm	127.84	371.45	67.64	219.87
	d < 100 nm	72.47	294.10	38.74	136.72
cinnamon soil colloids	d < 2 μm	141.23	439.20	78.29	244.97
	d < 1 μm	131.67	372.07	75.84	231.64
	d < 100 nm	85.48	312.25	47.84	158.99

556 Note: D_{10}, D_{50} and D_{90} represent diameter of particles with a cumulative distribution of 10%, 50% and
557 90%, respectively.
558

https://doi.org/10.5194/egusphere-2024-1266
Preprint. Discussion started: 11 June 2024

559 **Table 2** The physiochemical properties of Lou soil and cinnamon soil colloids

Soil colloids	Colloidal fractions	Yield (%)	Total carbon content ($g \cdot kg^{-1}$)	Organic carbon content ($g \cdot kg^{-1}$)	$CaCO_3$ content ($g \cdot kg^{-1}$)	Specific surface area ($m^2 \cdot g^{-1}$)
Lou soil colloids	$d < 2$ μm	25.12	20.9	10.9	10.0	65.37
	$d < 1$ μm	18.76	20.7	10.9	9.8	72.99
	$d < 100$ nm	6.32	58.2	27.4	30.8	45.28
cinnamon soil colloids	$d < 2$ μm	23.17	24.0	11.7	12.3	49.99
	$d < 1$ μm	16.20	22.3	12.8	9.5	61.88
	$d < 100$ nm	4.70	76.3	28.3	48.0	34.53

560

https://doi.org/10.5194/egusphere-2024-1266
Preprint. Discussion started: 11 June 2024

561 **Table 3** The dominant clay minerals of Lou soil and cinnamon soil colloidal fractions (shown
562 in mass fraction, %)

Soil colloids	Colloidal fractions	Illite	Kaolinite	Chlorite	Vermiculite
Lou soil colloids	$d < 2$ μm	34	23	4	9
	$d < 1$ μm	30	22	7	11
	$d < 100$ nm	37	14	16	3
Cinnamon soil colloids	$d < 2$ μm	24	22	29	16
	$d < 1$ μm	31	19	25	12
	$d < 100$ nm	37	16	17	5

563

https://doi.org/10.5194/egusphere-2024-1266
Preprint. Discussion started: 11 June 2024

564 **Table 4** The aggregation rates of Lou soil and cinnamon soil colloids

Soil colloids	Colloidal fractions	Aggregation rate		Fractal dimension	
		In 50 mmol·L^{-1} NaCl (nm·min^{-1})	In 1 mmol·L^{-1} $CaCl_2$ (nm·min^{-1})	Na	Ca
Lou soil colloids	d < 2 μm	19.46	12.01	1.69 ± 0.19	1.33 ± 0.26
	d < 1 μm	14.91	11.48	1.75 ± 0.06	1.52 ± 0.19
	d < 100 nm	7.72	9.97	1.71 ± 0.26	1.68 ± 0.13
Cinnamon soil colloids	d < 2 μm	8.98	8.22	1.30 ± 0.17	1.36 ± 0.17
	d < 1 μm	7.15	7.33	1.71 ± 0.24	1.30 ± 0.31
	d < 100 nm	3.95	5.22	1.52 ± 0.22	1.58 ± 0.19

565

https://doi.org/10.5194/egusphere-2024-1266
Preprint. Discussion started: 11 June 2024

Figure captions

Fig. 1. The photoelectron spectrum C1s and O1s peak diagram of Lou soil and cinnamon soil colloids. C1s of Lou soil colloids, a. $d < 2$ μm, b. $d < 1$ μm, c. $d < 100$ nm; C1s of cinnamon soil colloids, d. $d < 2$ μm, e. $d < 1$ μm, f. $d < 100$ nm; O1s of Lou soil colloids, g. $d < 2$ μm, h. $d < 1$ μm, i. $d < 100$ nm; O1s of cinnamon soil colloids, j. $d < 2$ μm, k. $d < 1$ μm, l. $d < 100$ nm.

Fig. 2. The zeta potential of Lou soil (a) and cinnamon soil (b) colloids of $d < 2$ μm, < 1 μm, and < 100 nm at different pH

Fig. 3. The CCCs of Lou soil (a) and cinnamon soil (b) colloids of $d < 2$ μm, < 1 μm, and < 100 nm in NaCl solution

Fig. 4. The CCC of Lou soil (a) and cinnamon soil (b) colloids of $d < 2$ μm, < 1 μm, and < 100 nm in CaCl2 solution

https://doi.org/10.5194/egusphere-2024-1266
Preprint. Discussion started: 11 June 2024

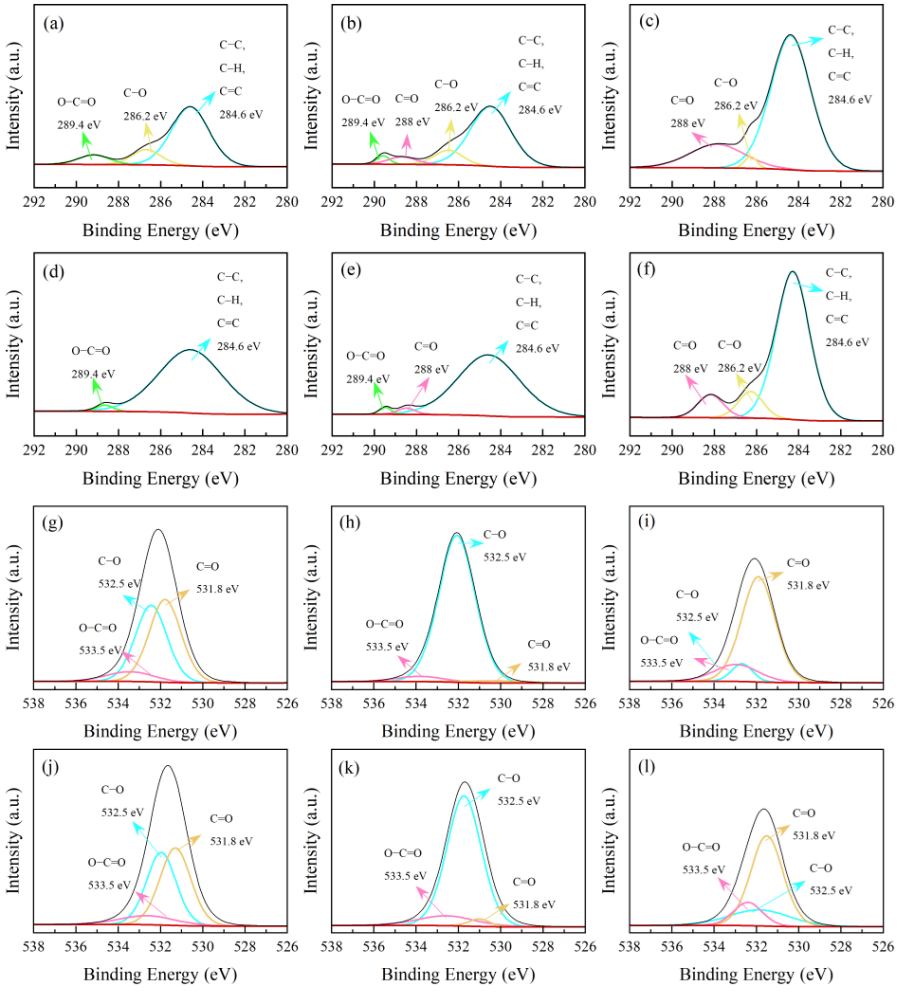

Fig. 1 The photoelectron spectrum C1s and O1s peak diagram of Lou soil and cinnamon soil colloids. C1s of Lou soil colloids, (a). $d < 2$ μm, (b). $d < 1$ μm, (c). $d < 100$ nm; C1s of cinnamon soil colloids, (d). $d < 2$ μm, (e). $d < 1$ μm, (f). $d < 100$ nm; O1s of Lou soil colloids, (g). $d < 2$ μm, (h). $d < 1$ μm, (i). $d < 100$ nm; O1s of cinnamon soil colloids, (j). $d < 2$ μm, (k). $d < 1$ μm, (l). $d < 100$ nm.

https://doi.org/10.5194/egusphere-2024-1266
Preprint. Discussion started: 11 June 2024

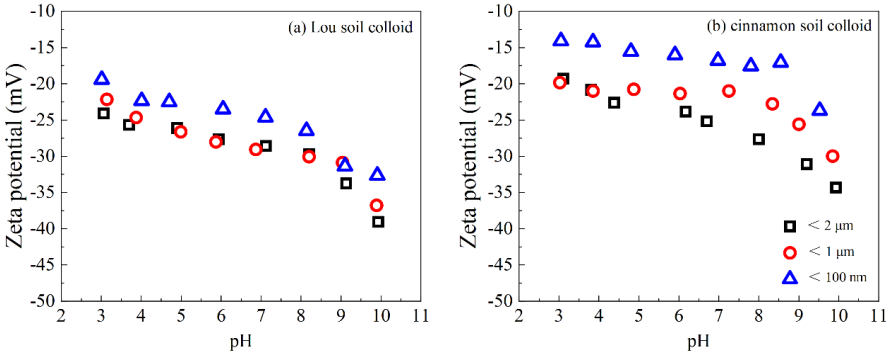

585

586 **Fig. 2** The zeta potential of Lou soil (a) and cinnamon soil (b) colloids of d < 2 μm, < 1 μm,
587 and < 100 nm at different pH

588

https://doi.org/10.5194/egusphere-2024-1266
Preprint. Discussion started: 11 June 2024

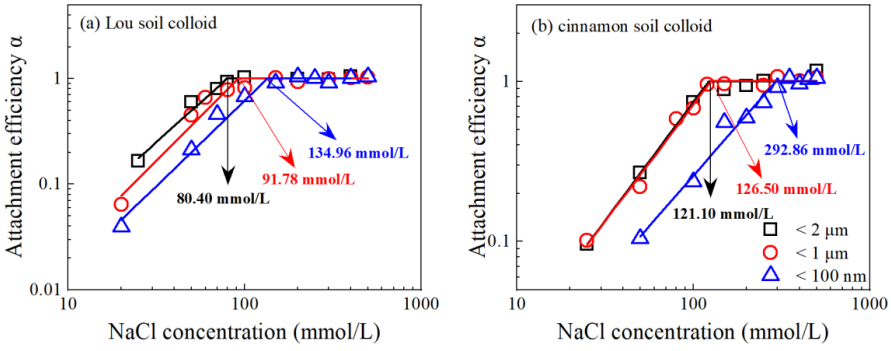

Fig. 3 The CCCs of Lou soil (a) and cinnamon soil (b) colloids of d < 2 μm, < 1 μm, and < 100 nm in NaCl solution

https://doi.org/10.5194/egusphere-2024-1266
Preprint. Discussion started: 11 June 2024

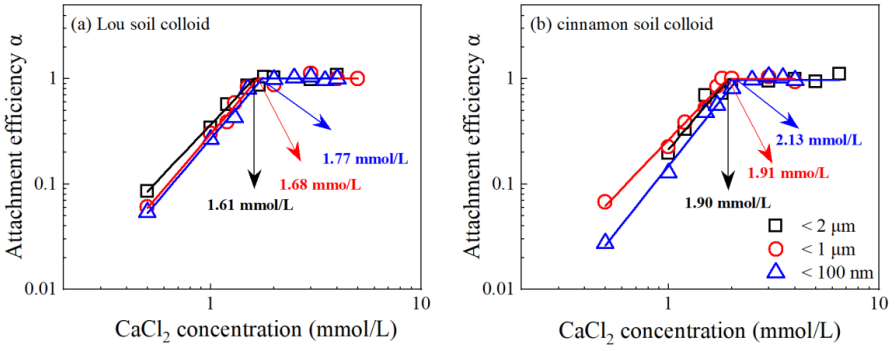

593

594 **Fig. 4** The CCC of Lou soil (a) and cinnamon soil (b) colloids of d < 2 μm, < 1 μm, and < 100
595 nm in $CaCl_2$ solution。